Band-gap renormalization and excitonic binding in T-shaped quantum wires

M. Stopa*
Tarucha Mesoscopic Project, ERATO-JST, 4S-308S NTT Atsugi Research and Development Center, 3-1 Morinosato Wakamiya, Atsugi-shi 243-0198 Kanagawa-ken, Japan

(Received 26 August 1999; revised manuscript received 19 July 2000; published 23 April 2001)

We calculate the electronic structure for a modulation doped and gated T-shaped quantum wire using density functional theory. We calculate the band-gap renormalization as a function of the density of conduction band electrons, induced by the donor layer and/or the gate, for the translationally invariant wire, incorporating all growth and geometric properties of the structure completely. We show that most of the band-gap renormalization arises from exchange-correlation effects, but that a small shift also results from the difference of wave function evolution between electrons and holes. We calculate the binding energy of excitons in a finite length wire using a simpler, cylindrical geometry. For a single hole and a one-dimensional electron gas of density n_e, screening of the exciton binding energy is shown to approximately compensate for band-gap renormalization, suggesting that the recombination energy remains approximately constant with n_e, in agreement with experiment. We find that the nature of screening, as treated within our nonlinear model, is significantly different from that of the various linear screening treatments, and the orthogonality of free carrier states with the bound electron states has a profound effect on the screening charge. In particular, we find no Mott transition. Rather, the electron and hole remain bound for all densities up to $\sim 3\times 10^6$ cm^{-1} and, as n_e increases from zero, trion and even ''quadron'' formation becomes allowed.

DOI: 10.1103/PhysRevB.63.195312 PACS number(s): 73.21.−b, 71.35.−y, 78.66.−w, 73.23.−b

I. INTRODUCTION

The gap in a semiconductor heterostructure between conduction and valence bands, and the interaction between electrons in the one and holes in the other, are known to depend in a complicated fashion on the presence of mobile charges.[1–3] The interpretation of optical experiments in doped semiconductor quantum wires,[4,5] for example, must invoke the variation of band edges due to many-body and geometrical effects, the ''redshift'' associated with electron-hole binding into excitons, and finally the reduction of the exciton binding energy due to screening by free carriers.

Theoretical description of band-gap renormalization (BGR) and exciton formation and screening is frequently addressed with a many-body formalism.[6–8] Within this framework, the contributions of both electron-phonon and electron-electron self-energies to BGR,[9] as well as the influence of dynamical screening on the exciton binding energy, can be studied. The many-body treatment, however, has the disadvantage that for BGR it commonly ignores geometrical factors, such as the quantum confined Stark effect,[10] whose relevance is structure specific. Furthermore, in the exciton problem, many-body theory treats screening within the linear approximation and, generally, the influence of the bound electron on the free electrons is not fully included. In particular, the orthogonality of the free electron states with the bound state, which increases in importance in lower dimensional systems, is typically not included.[11]

A different formalism without these shortcomings, albeit one that forsakes the electron-phonon interaction, is that of density functional theory (DFT).[12] Within DFT the ground state energy of an interacting many-particle system is known to be given rigorously by a functional of the density. The essential problem of DFT is that this functional is unknown and the components beyond kinetic and direct electrostatic energy are isolated into an ''exchange-correlation'' functional which must be approximated radically. Typically, the limit wherein the density varies adiabatically, known as the local density approximation (LDA), is assumed. Nonetheless, successful treatments of a wide class of systems, from atoms and molecules to solids and heterostructures, abound in the literature. It is the purpose of this paper to provide a theoretical description of BGR and exciton screening, applied particularly to semiconductor quantum wires (QW's), within DFT.

We are interested in quantitative comparison with optical experiments on T-shaped quantum wires (TQW's) in the presence of a one-dimensional gas of electrons (1DEG) with 1D density n_e, induced in the conduction band via a combination of modulation doping and gating.[13] By way of warning, this one-component plasma contrasts with the many studies that focus on intrinsic QW's wherein an overall charge neutral electron-hole plasma is generated entirely through photoexcitation. In our case photoexcitation is assumed to provide a small number of holes (which we take as a single hole) and to have a negligible effect on the density of conduction band electrons.

We evaluate the band structure of a TQW in two steps. In the first step (Sec. II) we consider a realistic model of a cross section of a TQW, shown in Fig. 1, and solve self-consistently for the electronic structure of the subbands, as a function of the gate voltage, assuming translational invariance along the wire. Material-specific effective masses and band offsets, as well as the actual growth profiles and doping densities of the structure, are included. The exciton problem is treated in the second step (Sec. III) by a simplified, cylindrical model of a quantum wire which we take to be of finite length. Thereby we explicitly break translational invariance. In this portion of the calculation we employ the results of Sec. II to estimate a reasonable lateral confinement param-

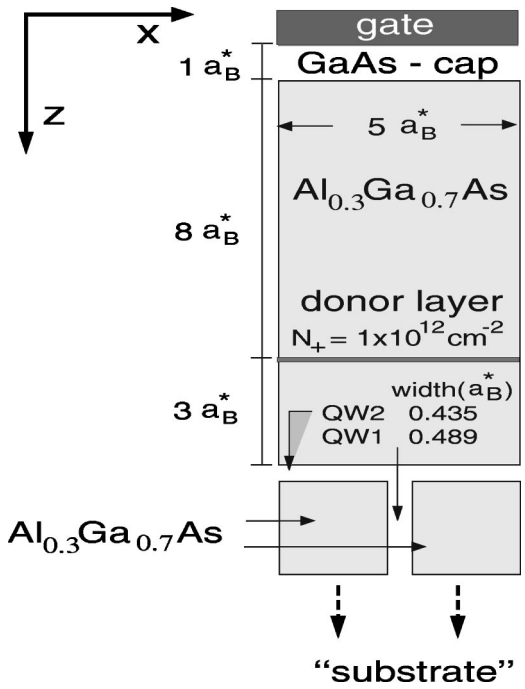

FIG. 1. Schematic of T-shaped quantum wire cross section.

eter. Thus the philosophy of the calculation is that the exciton formation and its screening represent an additive correction to the translationally invariant band structure of step 1. This exciton effect can be analyzed within a single-subband generic wire model so long as the effects of lateral confinement are correctly borrowed from the more faithful, albeit 2D, calculation in step 1.

Among our main results for the translationally invariant band structure (Sec. II) are the following. (1) We find a BGR as a function of n_e with comparable order of magnitude to that derived within many-body theory. (2) One small ($\sim$20%) component of this BGR arises from a variation of the lowest electron subband eigenfunction with n_e. Specifically, at higher n_e the lowest electronic wave function spreads somewhat along the overgrowth interface (throughout QW2 in Fig. 1, x direction) whereas it is more strongly confined at the junction (i.e., the intersection of the two wells) at lower n_e. The hole wave function, by contrast, never spreads appreciably along x. (3) The stability of the hole eigenstate at the junction is dependent on the boundary conditions used for large z (see Fig. 1). If the chemical potential is pinned to an assumed background donor density in the substrate (we use the term ''substrate'' to denote the region far from the donor plane, i.e., large z; see Fig. 1), then the hole bound state becomes a resonance which is metastable to escape into the substrate. On the other hand, when the substrate is treated as exactly electrically neutral (or pinned to acceptors) the hole state at the junction is stable. (4) For the specific dimensions and compositions that we consider[13] the wires are predominantly one dimensional with filling of no more than two subbands and spreading of the density into QW2 generally less than $\sim$15% of the total density.

Regarding the exciton problem (Sec. III), we find the following. (1) The exciton binding energy weakens considerably as the 1DEG density is turned on, but never vanishes completely. (2) The requirement of orthogonality between the bound electron eigenfunction and those of the screening electrons leads to an *antiscreening* of the exciton, such that the density of free electrons in the vicinity of the hole is depressed. This effectively positive charge raises the energy of the hole while the energy of the electron actually becomes more negative and its localization about the hole increases with density.

Finally, the contributions of the band-gap renormalization and the exciton screening tend to cancel and, consistent with experiments, the recombination energy remains relatively constant with n_e. This result is plotted in Fig. 6 but discussed at the end of Sec. III.

We principally employ effective atomic units wherein 1 Ry$^*=m^*e^4/2\hbar^2\kappa^2\approx 5.25$ meV and $1a_B^*=\hbar^2\kappa/m^*e^2 \approx 100$ Å. For comparison with experiments we also use cm^{-1}, where $1a_B^{*-1}\approx 10^6$ cm^{-1}. Figure 6 below, which gives the trend of the complete band gap with n_e, is presented in meV in order to be consistent with standard practice and also for comparison to experimental findings to be presented in a companion paper.[13]

II. TRANSLATIONALLY INVARIANT WIRE: BGR

We calculate the electronic structure of the GaAs-$Al_xGa_{1-x}As$ TQW's by solving Schrödinger and Poisson equations self-consistently,[14] within a region illustrated in Fig. 1, for the conduction band electrons, and by including exchange and correlation in the local density approximation.[12] There are numerous calculations of BGR in lower dimensional systems which employ many-body theory to determine the self-energy correction to the subbands from exchange and correlation effects.[15,16] In DFT a band-gap renormalization arises as follows. First, variations in the electrostatic potential tend to affect both bands equally except for kinematic effects like the quantum confined Stark effect,[10] where the electron wave function is centered on a different spatial location (at a different potential) than that of the hole. By contrast, exchange and correlation effects lower the energy of electrons in proportion to n_e, the electron density, and raise the energy of holes in proportion to n_h, the hole density, producing an overall shrinkage of the band gap. For the one-component plasma considered here, therefore, the exchange-correlation potential acts only on the conduction band electrons, since $n_h\approx 0$.

One advantage of our procedure is that, while many-body calculations in principle begin from wave functions and subband eigenenergies derived from some Hartree calculation, the variation of these properties with density and the aforementioned kinematical corrections to the band gap are usually ignored. By contrast, DFT automatically includes these. Furthermore, the separate contributions from kinematic effects as opposed to exchange and correlation are easily isolated (to first order) by performing a calculation without the exchange-correlation potential (i.e., Hartree only).

We employ the parametrization of Ceperley and Alder[17] for the density-dependent, exchange-correlation potential

$V_{xc}(n(\mathbf{x}))$. Taking y as the translationally invariant direction (see Fig. 1), the Schrödinger equation in the x-z plane ($k_y=0$) reads

$$\left[-\nabla\frac{1}{2m^*(x,z)}\nabla+V_C(x,z)+e\phi(x,z)+V_{xc}(n(x,z))\right]\psi_n(x,z)=E_e^n\psi_n(x,z), \quad (1)$$

where $V_C(x,z)$ is the conduction band offset,[18] which depends only on the local aluminum concentration η (we use the symbol η instead of the standard x to avoid confusion with the coordinate x), the 2D eigenfunctions and eigenvalues are given by $\psi_n(x,z)$ and E_n, respectively, and the electrostatic potential is $\phi(x,z)$. Also in Eq. (1) the level index is n, and the subscript e refers to electrons in the conduction band whereas for holes we use E_h^n. The eigenstates are abbreviated below as en and hn for electrons and holes, respectively. Periodic boundary conditions are taken at $x=\pm a/2$ where $a=5a_B^*$ is the period of the TQW superlattice as fabricated.[13] The effective mass dependence on position arises through its dependence on η.[18] In the specific device we consider, all regions have either $\eta=0$ (pure GaAs) or else $\eta=0.3$ for the barrier regions. We ignore interface grading effects as well as image effects, taking the dielectric constant as $\kappa=12.5$ everywhere.

For the solution of Poisson's equation we also assume periodic boundary conditions at the x borders. For the surface $z=0$ we simulate the surface metal gate in the standard fashion[14] by Dirichlet boundary conditions which fix the gate potential modulo an offset of 0.8 eV for the Schottky barrier. Variation of the electron sheet density in the overgrowth well N_e (or, equivalently, the 1D density n_e) is accomplished by biasing this surface gate. Other experimental methods for varying n_e include illumination or a variation of the thickness of the spacer between the modulation doping layer and the overgrowth well. While we have modeled each of these methods independently, in fact in each case there is an approximately homogeneous sheet (or sheets) of positive charge balancing the electronic charge in the wire/well and the difference in the electronic structure between the various methods, *for a given resultant* n_e, is negligible. Thus here we actually vary a surface gate voltage to change density, but in displaying the results it is sufficient just to plot variables versus n_e.

For large z we find, as noted, that the solution for the holes is sensitive to the asymptotic value of the potential. Generally, we assume Neumann boundary conditions, which is equivalent to assuming complete neutrality of the substrate. However, we discuss below the nature of the hole metastable state in the case where the chemical potential is pinned to a shallow donor level at large z.

Since the modulation doping is n type, the Fermi level is close to the conduction band throughout the device. Furthermore, since even during photoluminescence measurements the excitation power is very low, we ignore the valence band contribution to the charge density. Therefore, the total density that enters the Poisson equation is given as

$$\rho(x,z)=N_+(x,z)+n(x,z), \quad (2)$$

where $n(x,z)$ is the density of conduction band electrons only, and where the charge density of ionized donors is $N_+(x,z)$. The conduction band electron density is given in the well regions by

$$n(x,z)=\int dk_y \sum_n f(\mu-k_y^2-E_n)|\psi_n(x,z)|^2, \quad (3)$$

where f is the Fermi function, μ is the chemical potential (assumed constant throughout the device and taken as the zero of energy), and k_y^2 is the kinetic energy of motion in the y direction. We also employ a Thomas-Fermi approximation for the density of electrons in the barrier regions away from the wells. Finally, we assume temperature $T=4$ K.

We find little difference in the results whether the donors, which are silicon atom DX centers,[19] are placed in thermal equilibrium with the electron gas or are treated as a simple sheet of positive charge with fixed areal density. Insofar as at low temperatures the latter approximation is more physical, we use this assumption in the calculations discussed in this paper.

Upon obtaining a self-consistent solution of the Schrödinger and Poisson equations for conduction band electrons, we calculate the hole eigenfunctions with the potential

$$V_h(x,z)=V_V(x,z)-e\phi(x,z), \quad (4)$$

where now $\phi(x,z)$ is the electrostatic potential that solves the self-consistent problem above. The valence band offset $V_V(x,z)$ also depends on the aluminum concentration. We assume a band-gap offset parameter $Q_e=0.6$. We treat the holes in the simplest approximation, assuming a single, heavy-hole isotropic effective mass which depends only on aluminum concentration; specifically, $m_h^*(\mathrm{GaAs})=0.377m_0$ and $m_h^*(\mathrm{Al_{0.3}Ga_{0.7}As})=0.403m_0$.[20]

To summarize therefore and to make the context of this calculation clear, we are interested principally in the BGR as a function of n_e, the integral over x and z of $n(x,z)$, which we imagine to be modulated experimentally with an electrostatic gate on the overgrowth surface.[13] Thus we solve the evolving self-consistent electronic structure assuming the chemical potential to be far from the valence band (i.e., no holes). We solve for the hole subbands as a one-particle problem after solving the electronic structure at given n_e, using the resultant electrostatic potential. We use a simplified band structure for the holes, in contrast to Ref. 21, which employs the full, four-band Luttinger Hamiltonian but which assumes $n_e=0$.

A. Electronic structure

The parameters for the calculation are summarized in the schematic Fig. 1. We follow Ref. 21 by designating the overgrowth quantum well as ''QW2'' and the initial growth well as ''QW1.''

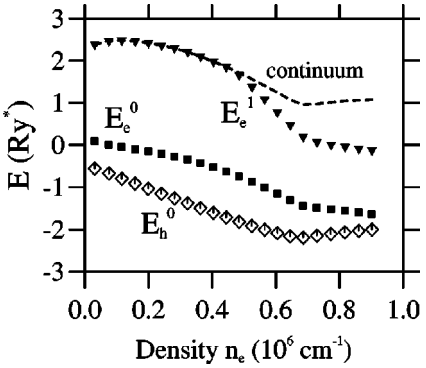

FIG. 2. Subband energies vs wire 1D density for electron (e) and hole (h). Electron levels measured with respect to Fermi surface; hole level with respect to escape to substrate. Electron continuum begins at dashed line. Filling of E_e^1 begins at $n_e \sim 0.5$.

The structure of the subbands of conduction band electrons as a function of n_e is shown in Fig. 2. The zero of energy for the electrons is the Fermi energy E_F (the plotted hole energy is discussed further below). In the higher density regime a second subband, which has concentration in the interwire QW2 region (cf. Fig. 4 below), is occupied. The region marked ''continuum'' corresponds to the beginning of a dense set of states which are asymptotically free to escape into the substrate (i.e., along QW1, which runs in the $+z$ direction). This is so because QW1 is wider than QW2, and the electrostatic advantage of proximity to the positive dopants in QW2 is overcome by the additional confinement energy there. Nonetheless, the spreading of the *occupied* states, when the total density is increased, occurs within QW2 (so as to compensate the positive charge of the donors and gate).

It is noteworthy that for $n_e \gtrsim 0.5 a_B^{*-1}$ ($\approx 0.5\times 10^6$ cm^{-1}), there are two subbands that are below the continuum, in contrast to the situation for lower n_e where only a single bound state exists. This is also consistent with the bare ($n_e = 0$) TQW studied in Ref. 21, which had a nearly identical aspect ratio (i.e., ratio of well widths) and exhibited only a single state separate from the continuum. The estimate there of a separation between E_e^0 and continuum of ~ 15 meV is also consistent with our slightly lower value of ~ 13 meV. Interestingly, this separation remains approximately constant (Fig. 2) as n_e is increased, until E_e^1 drops down from the continuum and begins to fill.

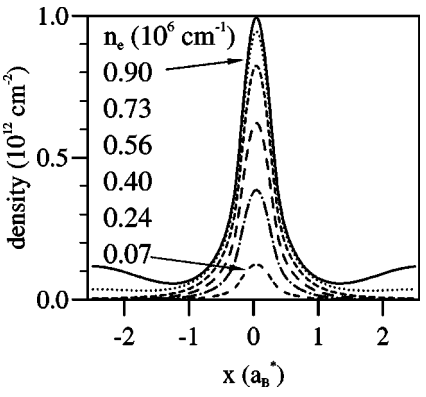

FIG. 3. Areal density (integrated along z) vs x for various total wire densities. Confinement to wire almost complete below $n_e \sim 0.6$. For highest n_e interwire density develops a subsidiary maximum at $\pm 2.5 a_B^*$.

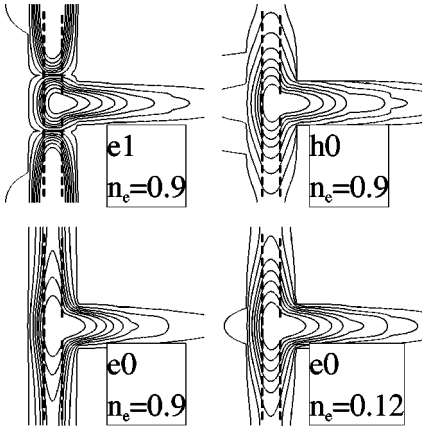

FIG. 4. Wave functions (moduli squared) showing spreading of e0 as n_e increases from 0.12×10^6 cm^{-1} (lower right) to 0.9×10^6 cm^{-1} (lower left). First excited electron state shows *two* nodes along x (upper left). Hole ground state (upper right) unchanging and strongly confined at junction.

In Fig. 3 we have plotted the 2D surface density as a function of x for various total n_e. As n_e approaches 1×10^6 cm^{-1} some spreading of the density away from the T junction occurs. This results both from the occupation of $e1$ and also from slight wave function spreading of $e0$ (cf. Fig. 4). Note, however, that, rather than spreading smoothly out from the wire, the density achieves a local maximum at an interwire minimum in the potential (at $\pm 2.5 a_B^*$, which, due to periodicity, are equivalent points), analogous to the electrostatic potential minima in the barriers of a semiconductor superlattice. Here, however, the effect is both electrostatic and quantum mechanical. The symmetry in x about the center of the junction and the periodic boundary conditions imply that the wave functions must have either local maxima or minima at the boundaries. Note, in Fig. 4, where the moduli squared of the eigenfunctions are plotted, that the subband $e1$ has *two* nodes along the x direction (i.e., along QW2). For different parameters (not shown), such as for a wider QW2 or much higher n_e, a state with a single node at the T junction is lower in energy. But in this regime the attractiveness of the T junction is sufficient to stabilize the even node state.

The spreading of $e0$ with increasing n_e observable in Fig. 4 is relevant to the evolution of the gap between conduction and valence bands. We will see below that the dominant portion of the BGR arises from exchange and correlation effects. Nonetheless, as noted in the Introduction, the difference between the evolution of electron and hole wave functions with n_e produces a kind of kinematic BGR as in the quantum confined Stark effect. Explicitly, the hole eigenfunction, which is shown in Fig. 4 only for $n_e = 0.9\times 10^6$ cm^{-1}, undergoes essentially no change with n_e over the n_e range of Fig. 2. Therefore the hole essentially tracks the electrostatic potential at the T junction. The electrons in $e0$, however, for increasing n_e, are able to lower

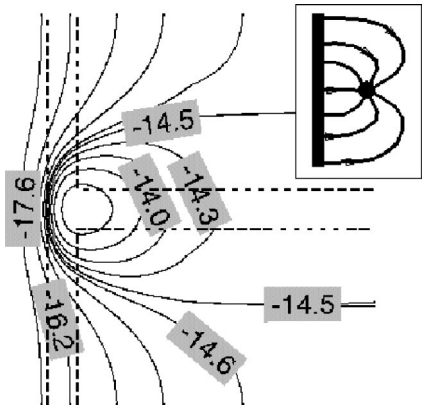

FIG. 5. Contour plot of electrostatic potential for $n_e = 0.9\times10^6$ cm^{-1}. Schematic illustrates field lines, which help to localize hole at junction.

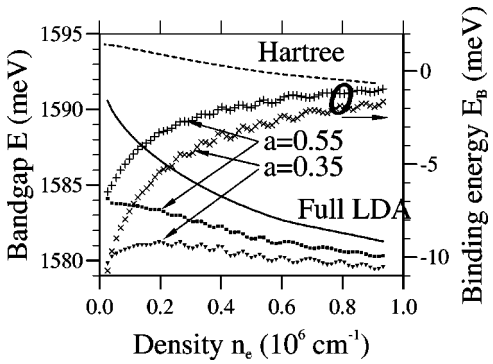

FIG. 6. Band-gap renormalization for full LDA (solid) and for pure Hartree (dashed), here in meV, as a function of density. Exciton binding energies for wire radius $a = 0.55a_B^*$ (pluses) and $a = 0.35a_B^*$ (crosses) and LDA band gap corrected for excitonic energy as squares and triangles, respectively.

their energy by spreading along QW2. This implies a redshift in the band gap which emerges even in the absence of exchange-correlation effects (see the Hartree results in Fig. 6 below).

B. Hole states

The stability of the hole state at the T junction depends weakly on the chosen boundary conditions for the Poisson equation at large *z*. If we pin the chemical potential to an assumed shallow donor level at large *z*, a common assumption, the hole state at the T junction is merely metastable, and escape, through a long, shallow barrier, to the substrate is energetically preferred. Assuming Neumann boundary conditions, or ''flat bands'' at large *z*, on the other hand, results in a true bound state. Dynamically, the difference between ''pinned band'' and flat band conditions is mostly inconsequential for holes photogenerated at the junction. For any reasonable background (i.e., unintentional) donor density, the barrier to escape of the hole is too large and the hole will remain and, presumably, recombine in the wire. Furthermore, the hole will induce an image in the electron gas which will cause further electrostatic binding to the wire region. A similar effect of holes bound to a 2DEG has been discussed recently in Ref. 22.

For holes generated in the substrate, far from the wire, however, the dynamics of the diffusion of holes into the wire region can be realistically expected to depend on the band shape as reflected in this dichotomy over boundary conditions. Generally, fewer background donors are favorable to hole diffusion from substrate into wire.

Even for pinned band conditions the basic charge distribution near the wire establishes a purely electrostatic barrier to hole escape, as seen in Fig. 5. Here we plot the 2D electrostatic potential for $n_e = 0.9\times10^6$ cm^{-1}. The potential contour principally derives from a plane of positive charge (the donor layer) and the line of negative charge in the wire. This results in an electrostatic potential hill near the junction (to which holes are attracted). Thus the hole has at least a long shallow barrier to escape even before considering the quantum effect that further binds the hole to the junction.

In Fig. 2 we plotted the energy of the first hole subband E_h^0 versus n_e. In this case we used Neumann boundary conditions for Poisson's equation at large *z* and the energy zero for E_h^0 is the electrostatic potential at large *z* added to the confinement energy of QW1; in other words it is the energy required to escape to the substrate continuum. Here we see that the state is stable, and not merely metastable (i.e., the energy is negative). Further, the increase in the binding with n_e (up to $n_e \sim 0.6\times10^6$ cm^{-1}) arises from the strengthening of the electrostatic potential minimum (for holes) shown in Fig. 5.

C. Band gap

The band gap in the heterostructure depends upon the assumed intrinsic band gap in the host materials GaAs and $Al_xGa_{1-x}As$, which, as noted, we have taken from the literature.[18] The band-gap variation with n_e is obtained from the sum of the lowest subband energies for the electron and the hole, each measured with respect to the GaAs band edge at any common point and then added to the intrinsic band gap. Figure 6 illustrates the variation of the band gap as a function of n_e. The rapid change for small n_e for the full LDA calculation derives from the form of the exchange-correlation potential. The exchange energy alone, for comparison, is proportional to the Fermi momentum $k_F = \sqrt{E_F}$.[23] The overall order of magnitude and shape of the BGR are consistent with the results of calculations within the *GW* approximation.[9] However, since the authors of Ref. 9 assumed a neutral, two-component plasma, the results are not quantitatively comparable.

In Fig. 6 we also plot the BGR for the case where the exchange-correlation potential is turned off, that is, for pure Hartree. Here the band gap still varies, albeit much less, with n_e. The origin of the shift, alluded to in the discussion of Fig. 4, is the variation of the wave function of the electron with n_e, which gives a kinematic component to its energy, while the hole eigenstate is essentially dormant at the junction. This effect is a slight generalization of the quantum confined Stark effect, wherein the band gap is affected by an electric field, which is varied, between the electron location

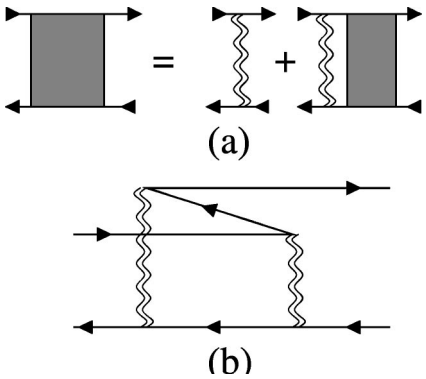

FIG. 7. (a) Standard ladder diagrams employed in solving Bethe-Salpeter equations. (b) Typically nonincluded ''crossed'' diagram, dependent on n_e, resulting from multiple scattering of a single electron from the hole.

and that of the hole. In our case the electron additionally shifts its location as the gate bias varies.

We postpone a discussion of the final result of Fig. 6, the behavior of the BGR when corrections for excitonic energy and screening are included, until after the next section.

III. EXCITON

A. Motivation

In the preceding section we implicitly assumed that, along the direction of the wire (y), the eigenstates of holes and electrons were plane waves. As a simple example, in the limit of a single electron and single hole, our assumed ''many-body'' state is of the form

$$\Psi(\mathbf{r}_h,\mathbf{r}_e)=\psi_e(x_e,z_e)e^{ik_e y_e}\psi_h(x_h,z_h)e^{ik_h y_h}, \qquad (5)$$

where the subscripts e and h denote electron and hole, respectively. This description ignores the exciton binding effect, which introduces a correlation between the hole position and that of (at least) one electron. The product of plane waves $e^{ik_e y_e}e^{ik_h y_h}$ admits no such correlation along the wire direction. Even if we continue to maintain, as we shall, the single-hole limit, the introduction of the excitonic effect is a considerable complication.

The standard treatment of this problem is via the Bethe-Salpeter equation.[7] However, this so-called ladder approximation employs several restrictions which we desire to go beyond. Specifically, as in most many-body theories, dielectric response is treated linearly, typically within the plasmon-pole approximation. Hence the low density limit is questionable. Additionally, the sum of ladder diagrams generally omits contributions from crossed diagrams (Fig. 7). Such terms depend on the density (in our case, the density of electrons) and represent quantum mechanical correlations in the electron gas induced by interaction with the hole. We will argue that such correlations, in the high density limit, are responsible for preventing the exciton state from merging with the continuum, and indeed promote the formation of multiple electron states bound to the hole (trions and ''quadrons'').

We are motivated by the work of Vinter[24] on binding of electrons to impurities in the presence of an electron gas, to examine the exciton problem via density functional theory. We emphasize, however, that our approach does not imply an infinite mass approximation for the hole. The primary ''approximation'' of DFT is to treat the wave function as a product of one-particle states and include exchange and correlation locally, through a potential. The nature of this approximation is seen most clearly when we consider the single-electron, single-hole limit (assuming purely 1D for the moment). In this case, the standard solution is to transform coordinates to relative ($\eta \equiv x_e - x_h$) and center of mass (X) motion, writing $\Psi(x_h,x_e)=\psi^{CM}(X)\psi^{x}(\eta)$. Correlation is thereby included precisely via the relative coordinate η. By contrast, as we discuss further below, DFT reduces in the two-particle limit simply to $\Psi(x_h,x_e)=\psi^{e}(x_e)\psi^{h}(x_h)$. Self-consistency does introduce correlation between x_h and x_e, but it is underestimated. It is in this limit where we expect our solution to be most inaccurate. The virtue of DFT is that it extends beyond the two-body problem, where the separation of variables and the exact solution are no longer available. Furthermore, as we show below, the deviation of the binding energy from the correct value is not so great as might be expected even in this limiting case. This is partly aided by the fact that the problem is one dimensional.

In addition to underestimating correlation in the two-particle limit, the product solution, by definition, discards center of mass motion. Furthermore, in order to actually calculate the binding of the electron and hole in the wire, i.e., the exciton interaction, the calculation must be restricted to a finite length of wire.[25] Computationally this results in the hole localizing at an essentially arbitrary point, bound to an accumulated electron cloud. However, at least in the two-body limit, according to the exact solution the exciton binding energy is *independent* of center of mass motion. Therefore, by placing the hole at rest we are making no approximation to the binding energy so long as our sample is large enough that boundary conditions do not affect the solution, which we have checked.

In summary, assuming a direct product solution underestimates correlations; a problem that is most conspicuous in the two-body limit. Confining the system to a finite wire, however, implies no further approximation, so long as L_y is taken sufficiently large. This is physically reasonable since natural size cutoffs, such as localization length and inelastic scattering length, are present in real systems and any theoretical result that depended on a truly infinite size of the system would be highly suspect.

A crucial element of our calculation is the treatment of the hole self-interaction. The exchange-correlation potential in DFT behaves much like the exchange term in Hartree-Fock theory. In both cases exchange reduces the interaction of pairs of electrons but more to the point it compensates for the interaction of an electron with itself. In Hartree-Fock theory this cancellation is exact; in DFT it is approximate, and some uncompensated self-interaction remains, a fact that has been well known for years. But since we have only a single hole, and since we are *calculating* its correlation with the electron gas (the excitonic effect), we should not include an

exchange-correlation potential for the hole. How, then, are we to compensate for the interaction of the hole with its own Coulomb field, even approximately?

One conceptually simple method to eliminate self-interaction from the Hartree problem for a finite fermion system would be to calculate a different electrostatic potential, and hence different Hamiltonian, for every electron. The potential experienced by each electron would then be calculated from the density of all other electrons, but not itself.[26] In the general case (typified, say, by the calculation of the electronic structure of an atom), it is unclear how to execute this, since one then has a different eigenvalue problem for each state. Obviously one cannot choose the ground state from each Hamiltonian. Does one choose the pth eigenfunction from the pth Hamiltonian? The problem is ultimately that the orthogonal set resulting from a single eigenvalue problem is lost.

However, it is just such an approach that we employ here. This is, in our case, unambiguous because we have two species of particles and for one of the species (the hole) we have only one member. Thus the hole eigenfunction is computed from the electrostatic potential arising from all charge other than the hole itself. The electron ''Kohn-Sham'' states are still calculated as usual from the total charge density, and the exchange-correlation potential is employed as usual to compensate (partially) for electron self-interaction.

In what follows we will begin by discussing the geometry of the model used in this portion of the calculation. The cylindrical wire that we utilize is chosen so that the three-dimensional problem can be simply reduced to a quasi-one-dimensional problem. The limitations of this approximation and its relationship to the transverse wave functions in Sec. II are discussed. We will then lay out the full system of equations and boundary conditions to be solved. Following this we discuss two instructive simplified cases of the problem. Both of these are based on an effective 1D pair interaction (as opposed to a solution of the full Poisson equation in 3D) for which we develop a convenient approximation. In the first we treat the electron gas via the Thomas-Fermi approximation, showing that the hole spontaneously localizes with a cloud of electrons nearby. In the second we examine quantitatively the two-body limit of DFT and compare the results to the exact solution employing the transformation to relative and center of mass coordinates, as discussed above. We then proceed to a presentation of the results of the full, self-consistent exciton calculation and apply those results additively to the band-gap energy of the previous section to obtain the overall trend of the luminescence energy with varying electron density.

B. Model geometry

In this section we employ a simplified geometry, shown in Fig. 8(a), for a single-mode, cylindrical quantum wire along direction y of radius a surrounded by a cylindrical metal gate at radius Λ whose potential U_{ext} is used to vary the electron density. The radial charge distribution of both electrons and holes is assumed to be given by a single Gaussian wave function $\xi(r)=(1/a)\sqrt{2/\pi}e^{-r^2/a^2}$. Clearly this approximation is valid only in the limit of a very strongly confined system. We believe that, even though our system is indeed strongly confined and the qualitative conclusions of this section are independent of this approximation, the primary factor that limits the numerical accuracy of our calculation is most likely this assumption.

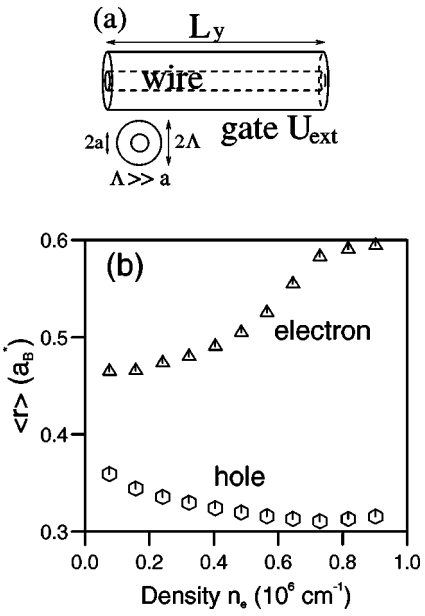

FIG. 8. (a) Schematic of cylindrical wire for model exciton calculation. Radial charge distribution of hole and electron taken as single Gaussian. Drawing not to scale: $\Lambda \gtrsim 10a$. (b) Radial spread of wave functions for lowest conduction and valence band states in T-shaped wire, as a function of total 1D density. Parameters correspond to Fig. 2.

In comparing with Sec. II we must choose a value of a that is consistent with the lateral spread of the electron and hole wave functions. We have calculated the radial spread of the lowest electron and hole eigenstates (cf. Fig. 4) for the TQW,

$$\langle r\rangle \equiv \int dx\, dz \quad \sqrt{x^2+z^2}\,|\psi_0(x,z)|^2, \tag{6}$$

and plotted the results, as a function of n_e, in Fig. 8(b). A distinct shift in $\langle r\rangle$ for the electron is seen near $n_e = 0.6\times 10^6$ cm^{-1}. This occurs around the filling of the second subband. This corresponds to the lateral (along the x direction) spreading mentioned in the discussion of Fig. 4. For the radial a parameter employed in this section, we choose various values between the exhibited range for the hole and the electron (typically we compute results for $a = 0.35a_B^*$, $0.45a_B^*$, and $0.55a_B^*$).

Finally, we find that for $L_y \approx 30a_B^*$ the eigenstates show negligible dependence on L_y. For example, the eigenvalues shown in Fig. 12 below show small fluctuations related to the discrete density of states, but they never exceed 0.05 Ry*.

C. Equations

The system of equations that we solve is presented below. The Schrödinger equations for the electron and hole, respectively, read

$$\left(-\frac{1}{2m_e}\frac{\partial^2}{\partial y^2} + V^e_{eff}(y) + \tilde{V}_{xc}(y) \right) \psi^e_p(y) = \varepsilon^e_p \psi^e_p(y),$$

$$\left(-\frac{1}{2m_h}\frac{\partial^2}{\partial y^2} + V^h_{eff}(y) \right) \psi^h_p(y) = \varepsilon^h_p \psi^h_p(y), \tag{7}$$

where the effective one-dimensional electrostatic potentials are determined from the three-dimensional electrostatic potentials as

$$V^{e,h}_{eff}(y) \equiv \int d^2r |\xi(r)|^2 e\phi_{e,h}(r,y). \tag{8}$$

The electrostatic potentials are determined from the full 3D Poisson equation, assuming azimuthal symmetry,

$$-\nabla^2 \phi_e(r,y) = \frac{4\pi}{\kappa}[\rho_e(r,y) + \rho_h(r,y)],$$

$$-\nabla^2 \phi_h(r,y) = \frac{4\pi}{\kappa}\rho_e(r,y). \tag{9}$$

We can also include an explicit background charge in the source terms of Eqs. (9); however, for the results discussed here we have changed the chemical potential and the effective background charge by means of the surrounding gate.

The density of electrons is determined from the eigenfunctions and eigenvalues of Schrödinger's equation,

$$\rho_e(r,y) = |\xi(r)|^2 \sum_{p=1}^{\infty} f(\mu - \varepsilon^e_p) |\psi^e_p(y)|^2, \tag{10}$$

where f is the Fermi function and μ is the chemical potential, which is usually taken as the energy zero of the problem. The hole density $\rho(r,y)$ is calculated similarly but with only a single eigenstate and a filling of unity.

For the electrons, the effective 1D exchange-correlation potential is obtained from the 3D form (see Sec. II) as

$$\tilde{V}_{xc}(y) = \int d^2r |\xi(r)|^2 V_{xc}(\rho_e(r,y)). \tag{11}$$

Equations (7) are solved with periodic boundary conditions on the interval $y \in [-L_y/2, L_y/2]$. The 3D Poisson equations are solved with Neumann conditions at $\pm L_y/2$ and with Dirichlet boundary conditions on the gate at $r = \Lambda$. We note that the Dirichlet boundary conditions on the gate imply a small, subtle error. By using, for the hole, the electrostatic potential computed without the hole charge $\rho_h(\mathbf{r})$ included, the image charge induced by the hole on the gate, with which the hole physically does interact, is absent. A more precise, though computationally taxing, approach would be to compute $\phi_h(r,y)$ from all the charge but then subtract $\int d^3r' \rho_h(\mathbf{r}') e/|\mathbf{r} - \mathbf{r}'|$, the potential of the hole in free space.

The binding energy E_B of the exciton is defined as the difference in the total energy between the case where the hole is localized, on the one hand, and the case where the single-hole charge is spread uniformly in y, a free hole, on the other hand. The total energy must include, in addition to the sum of occupied eigenvalues, a double-counting correction as well as the energy related to the gate. Furthermore, this gate energy is modified by the work supplied to the gate,[14,27] and is hence really a *free* energy. The overall expression for this free energy is thus

$$F(U_{ext}) = \varepsilon^1_h + \sum_p f(\mu - \varepsilon^e_p)\varepsilon^p_e - \frac{1}{2}\int d^3r \times [\rho_e(\mathbf{r})\phi_e(\mathbf{r}) + \rho_h(\mathbf{r})\phi_h(\mathbf{r})] + \int d^3r \rho_e(\mathbf{r}) \times [\varepsilon_{xc}(\rho_e(\mathbf{r})) - V_{xc}(\rho_e(\mathbf{r}))] - \frac{1}{2}QU_{ext}, \tag{12}$$

where Q is the total charge induced on the gate, determined by computing the normal derivative of the potential at the gate surface. Also, the third term on the right hand side of Eq. (12) is a form of double-counting correction for the exchange-correlation energy, where $\varepsilon_{xc}(\rho)$ is the exchange-correlation energy per particle of a homogeneous electron gas of density ρ.[12]

We note that one might write the total energy as simply the sum of occupied Kohn-Sham energies (including the hole) via Koopman's theorem. To lowest order, where only a single bound electron and the hole energies are changing appreciably, one could further estimate this as simply $F(U_{ext}) = \varepsilon^1_h + \varepsilon^1_e$. However these are both approximations and the correct formula, Eq. (12), must be used for all but heuristic purposes.

D. Thomas-Fermi model

To obtain a qualitative understanding of the results of the full self-consistent calculation we present here a calculation where the 1D electron gas is treated within the Thomas-Fermi approximation and the hole eigenstate is determined variationally. For this and the ensuing sections we do not solve the full 3D Poisson equation, but rather employ the effective 1D interaction. We further approximate this by a simple, practical form which is very convenient for calculation (for a similar model, see Ref. 28). With the assumed Gaussian wave functions in the transverse direction, the effective 1D Coulomb interaction is

$$V(y-y') = -\frac{e^2}{\kappa}\int d\rho \ \rho d\phi \int d\rho' \rho' d\phi' \times \frac{|\xi(\rho)|^2 |\xi(\rho')|^2}{\sqrt{(y-y')^2 + \rho^2 + \rho'^2 - 2\rho\rho' \cos(\phi - \phi')}}. \tag{13}$$

This integral can be easily performed numerically by writing the kernel as an expansion in modified Bessel functions.[29] The results can be empirically fitted to a function of the form

$$V(y-y') = \frac{e^2}{\kappa}\frac{A_1}{\sqrt{(y-y')^2 + A_2^2}}, \tag{14}$$

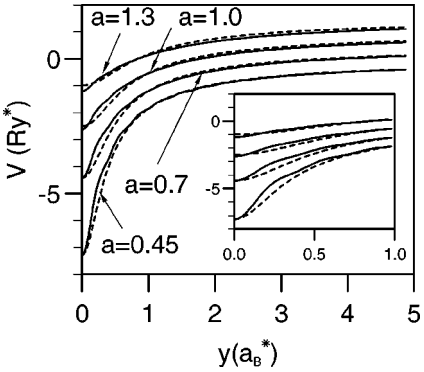

FIG. 9. Effective 1D potential curves versus y ($y'=0$ here) calculated according to Eq. (13) (solid) and the fitting function (dashed) from Eq. (14) using Eqs. (15) for the parameters A_1 and A_2, given a (listed on figure). Curves are offset vertically for clarity; offsets, from bottom to top, are 0, 0.5, 1.0, and 1.5 Ry*. Inset shows closeup near origin.

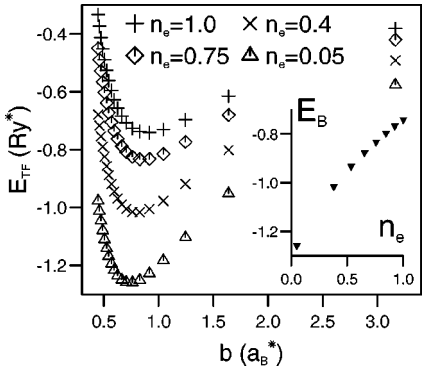

FIG. 10. Energy of hole in 1D Thomas-Fermi electron gas, including hole kinetic energy, as a function of hole wave function radius b for various electron densities (listed in 10^6 cm^{-1}). Wire width $a=0.45a_B^*$. Energy measured relative to state with $b=\infty$, i.e., with hole charge spread out uniformly. Inset shows energy minimum, i.e., binding energy, versus n_e. Variation of only 0.5 Ry*$\approx$3 meV is small compared to full quantum mechanical calculation (cf. Fig. 6).

where we find A_1 and A_2 as functions of the wave function parameter a,

$$A_1=-1.02+0.18a+0.015a^2,$$

$$A_2=0.0074+0.58a-0.11a^2, \tag{15}$$

where a is assumed to be given in a_B^*, A_1 is dimensionless, and A_2 is in a_B^* (thereby determining the dimensions of the constants). Figure 9 shows a comparison of the exact results from (13) and the fitting function (14) for various values of a. We find that Eq. (14) gives a reasonable approximation to Eq. (13) as long as a is in the range of $[0.25,2.0]a_B^*$.

Given an effective 1D pair potential, we will solve the problem of a single hole in a sea of electrons described by the Thomas-Fermi approximation, with the eigenstate of the hole given by a simple function with one variational parameter, that is,

$$\psi^h(y)=\left[\frac{2}{b^2\pi}\right]^{1/4}e^{-y^2/b^2}. \tag{16}$$

Note that this (1D) Gaussian ansatz for the binding of the hole along y can be distinguished from the Gaussian form of the 2D transverse wave function by the normalization factor.

For a given fixed hole wave function, i.e., a fixed b, the Thomas-Fermi problem consists of minimizing the following functional of the electron density $\rho(y)$:

$$E[\rho(r)]=\int dy\left[\frac{\hbar^2\pi^2}{24m_e}\rho^3(y)-\overline{\rho}(y)\int dy'|\psi^h(y)|^2\right.$$

$$\times V(y-y')+\frac{\overline{\rho}(y)}{2}\int dy'\overline{\rho}(y')$$

$$\left.\times V(y-y')-\mu\overline{\rho}(y)\right], \tag{17}$$

$$\frac{\delta E}{\delta\rho(y)}=0, \tag{18}$$

where $\overline{\rho}(y)\equiv\rho(y)-\rho_0$, with ρ_0 the background charge density, and where μ, a Lagrange multiplier, is the chemical potential. The variation Eq. (18) is trivial and leads to an integral equation for $\rho_{min}(y)$, the energy minimizing electron density, which is easily solved iteratively. To the resulting energy $E[\rho_{min}(y)]$ we add the kinetic energy of the hole $\hbar^2/2m_hb^2$ to obtain the Thomas-Fermi energy $E_{TF}(b)$ (Fig. 10). For the finite size wire, when b becomes very large, we must prevent the hole density from pouring outside the range $[-L_y/2,L_y/2]$ by renormalizing $\psi^h(y)$ such that the total hole charge in the wire remains unity.

The minimum energies $E_{TF}(b)$ are plotted in Fig. 10 versus b for several background charge densities, where $\rho_0=2\sqrt{2m_e\mu}/\pi\hbar$. The energy zero in the figure is $E_{TF}(\infty)$, i.e., the energy of the hole–TF-gas system when the hole charge is spread uniformly through the wire. The potential parameters, A_1 and A_2 are taken from Eq. (15) for a wire width $a=0.45a_B^*$. An exponential damping has also been included in the potential to simulate a screening gate, but the results are insensitive to the imposed screening length when it is substantially greater than the wire width. Clearly the overall energy is minimized at a finite b for all values of ρ_0. Comparison of these energies versus ρ_0 with the exciton binding energies from the full calculation (displayed in Fig. 6 and discussed below) shows an order of magnitude agreement, and a trend of weaker binding with increased μ, but otherwise the results are poor in comparison with the full calculation. The principal message here is that a one-dimensional quantum particle in a dielectric medium can be localized by the polarization cloud which it produces.[22] In the Thomas-Fermi model, no account is given of whether the screening electrons come from the top of the Fermi sea, in the form of scattering phase shifts, or the bottom of the Fermi sea, in the form of individual bound states. Clarification of this point in particular is one of the key points of the current study.

E. Two-body problem

In the limit of a single hole and single electron in an otherwise empty wire, if we employ again the effective 1D pair potential of the preceding section, the set of Eqs. (6)–(10) reduces to

$$\left(-\frac{1}{2m_e}\frac{\partial^2}{\partial y_e^2} + \int dy_h V(y_e - y_h)|\psi^h(y_h)|^2 \right)\psi^e(y_e) = E_e\psi^e(y_e),$$

$$\left(-\frac{1}{2m_h}\frac{\partial^2}{\partial y_h^2} + \int dy_e V(y_h - y_e)|\psi^e(y_e)|^2 \right)\psi^h(y_h) = E_h\psi^h(y_h), \tag{19}$$

where now there is no exchange-correlation potential for electrons. The total energy of the system, which in this approximation we call E_2, is given by

$$E_2 \equiv E_e + E_h - \frac{1}{2}\int dy[\rho_e(y)\phi_e(y) + \rho_h(y)\phi_h(y)], \tag{20}$$

where here, of course,

$$\rho_e(y) \equiv |\psi_e(y)|^2,$$
$$\rho_h(y) \equiv |\psi_h(y)|^2, \tag{21}$$

and

$$\phi_e(y) \equiv \int dy_h V(y - y_h)|\psi^h(y_h)|^2,$$
$$\phi_h(y) \equiv \int dy_e V(y_h - y)|\psi^e(y_e)|^2. \tag{22}$$

Please note that this result is the two-body limit of Eqs. (6)–(10) but that it also follows directly from the two-body Schrödinger equation with no other assumption than that the two-body wave function can be written as a product state: $\psi^e(y_e)\psi^h(y_h)$. Still, as noted above, in this two-body limit the product wave function constitutes a radical approximation in that each particle is assumed to be moving independently in the average field produced by the other.

The exact solution of the two-body problem is given by the separation of the two-particle Schrödinger equation into relative and center of mass coordinates[1] which, for our 1D problem, is written

$$\left[-\frac{1}{2\mu}\frac{\partial^2}{\partial \eta^2} + V(\eta) \right]\psi^x(\eta) = \left(E_x - \frac{\hbar K^2}{2M} \right)\psi^x(\eta), \tag{23}$$

where K is the momentum of the center of mass, with total mass $M = m_e + m_h$, η is the relative electron-hole coordinate, and here μ is the reduced mass. A comparison of the total energy obtained from the self-consistent solution of the set of equations (19) and the $K=0$ binding energy E_x obtained from the solution of Eq. (23) shows a deviation on the order of 25%, decreasing as the transverse extent of the wave function increases (Fig. 11). This is not so bad insofar as the *raison d'être* of density functional theory is not the solution of two-body problems. Mathematically, the fact that DFT is not a complete failure in this regime is reasonable in that the correct wave function, written in terms of η and X, could in principle be expanded in a *series* of products of functions of y_e and y_h. We are then retaining only the leading term of such a series, but we are calculating it self-consistently. Note, however, that in dimensions higher than one the accuracy of such a procedure is bound to decrease simply because the number of independent variables in which one must expand the wave function increases from two to four to six.

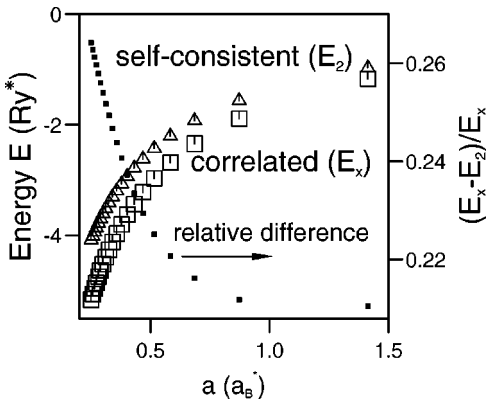

FIG. 11. Binding energy for two-body problem using correct separation of variables with correlation, E_x, and simple product ansatz from limiting case of DFT, E_2, as a function of a, radial wave function spread. Fractional difference in the range of 20 $-25\,\%$.

F. Results

We proceed now to exhibit the results of the full self-consistent calculation based on the solution of Eqs. (6)–(10).

In Fig. 12 we show E_B [see the definition in discussion prior to Eq. (12)] computed as a function of U_{ext} for $a = 0.35a_B^*, 0.45a_B^*$, and $0.55a_B^*$. Also plotted is the conduction band density n_e, which is here defined as the total number of conduction band electrons in the wire for the localized hole case, minus unity (the bound electron), divided by the wire length L_y. When the gate voltage becomes negative, all electrons become depleted from the wire and, below $U_{ext} = -1.0$ Ry*, the conduction electrons for the delocalized hole case shift from the wire to the gate. This explains the jump in E_B below depletion. The minimum of E_B occurs at the lowest density before this shift occurs, corresponding to a single electron in the wire. Clearly the minimum depends somewhat sensitively on the choice of a, and the binding can become quite strong for very narrow wires, as is well known.[30] Our empirical form of the effective 1D potential, Eq. (14), gives a good, intuitive understanding of this in that the parameter A_2 decreases with decreasing wire width (cf. also Fig. 11 for small a). Note that the small fluctuations visible in the energies result from the finite size L_y and the discreteness of the ''free'' states.

Of considerable interest is the absence of a binding to unbinding transition for the exciton. Even when we extend

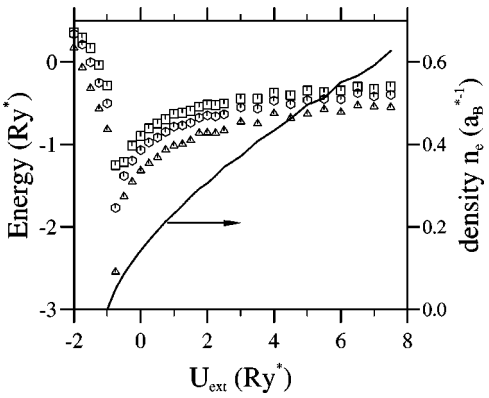

FIG. 12. Binding energy of exciton vs gate potential for $a=0.35a_B^*$ (triangles), $0.45a_B^*$ (hexagons), and $0.55a_B^*$ (boxes). Line gives corresponding n_e (see text for exact definition). Rise of energy below $n_e=0$ caused by shift of electronic charge to gate for delocalized hole case.

the density range to $>2a_B^{*-1}$ (i.e., $>2\times10^6$ cm^{-1}) and even for the widest charge distribution $a=0.55a_B^*$, the ground state remains bound (not shown). In fact, as shown in Fig. 13 (see also Fig. 14), a second electronic state becomes localized about the hole above $U_{ext}\approx1.25$ Ry*, corresponding to $n_e\approx0.2a_B^{*-1}$, thus forming a so-called trion.[31] Here we have plotted the (Kohn-Sham) level energies for the localized hole case, measured relative to the band edge far from the hole, so that an energy above zero indicates an asymptotically free particle. We find that for even higher densities, $>0.8a_B^{*-1}$, a third electron can become bound to the hole; a state which we refer to naturally as a ''quadron.''

It is important to note that the formation of such an electron-trion bound state would be impossible in vacuum, since it represents the binding of two negative charges. However, in our wire system charge neutrality is enforced by the metallic, constant potential of the surrounding cylinder. Furthermore, this background charge is treated as fully classical

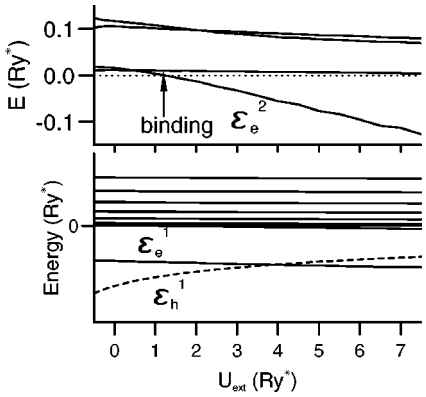

FIG. 13. Lower panel: discrete Kohn-Sham energy levels for electron (solid) and hole (dashed) vs gate voltage, $a=0.35a_B^*$. To lowest order exciton binding energy is $E_B\approx\varepsilon_e^1+\varepsilon_h^1$; hence binding weakens with increased U_{ext} (and n_e). Hole localizes two electrons above $U_{ext}\approx1$ Ry*. Upper panel: magnification near $E=0$ showing that second electron binds to hole to form trion at $U_{ext}\approx1.25$ Ry*.

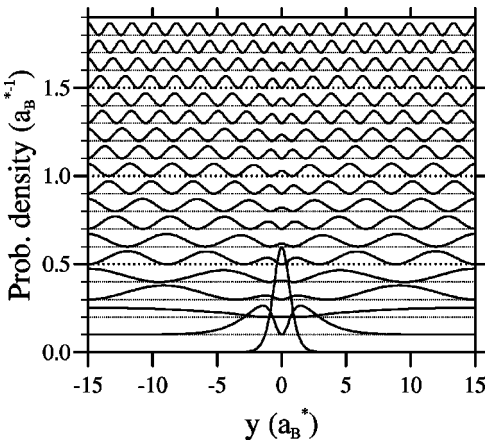

FIG. 14. Occupied electronic wave functions (moduli squared), states 1 through 19, $a=0.35a_B^*$, $n_e=0.6\times10^6$ cm^{-1}. Two states are localized near hole (at $y=0$). Orthogonality of remaining states to bound states suppresses screening charge density near hole.

— there is no Fermi wavelength in the metal to cut off screening at short distances. Electrons are added to the wire by increasing the positive potential on this gate, i.e., by adding positive charge. Since the orthogonality of the electrons to the bound electron reduces the probability density of successive states near the origin (see next paragraph and Fig. 14) and since the background charge is under no such constraint, there is a *net* increase of positive charge in the vicinity of the origin as density is increased. Of course, the positive charge resides on the external cylinder away from the 1DEG, so its effect is relatively weak. But eventually it is strong enough to bind an additional electron.

The most intriguing feature of the results in Fig. 13 is that, while the hole becomes more weakly bound, and consequently more spatially extended, the electrons, particularly the lowest state, become more strongly bound with increasing U_{ext} (and consequently increasing n_e). A similar result for electron binding to an ionized impurity in a 2DEG silicon inversion layer was found by Vinter.[24] This feature, which is related to the quadron binding just discussed, is rather counterintuitive, since one expects screening, by free electrons, of the interaction between hole and bound electron to weaken the attraction and separate the particles. Partially this result is understood as relating to the direct product nature of the exciton state when expressed in DFT, as opposed to the single composite state of the two-body or screened two-body problem. Thus the binding energy is not a single eigenvalue, or even the sum of two eigenvalues, but rather it must be understood as a difference between two interacting ground states. In other words, as is well known, care must be used when interpreting the meaning of the Kohn-Sham eigenvalues and eigenfunctions. Nonetheless, the decreased energy and increased localization of the lowest Kohn-Sham level seem puzzling. In Fig. 14 we show, for a relatively high density $n_e=0.6a_B^{*-1}$, the set of all occupied eigenfunctions (moduli squared). At this n_e the lowest two-electron states are localized near the hole at $y=0$. Note, however, that due to the restraint of orthogonality the densities of all other states in the vicinity of the hole are *suppressed*. Thus, while

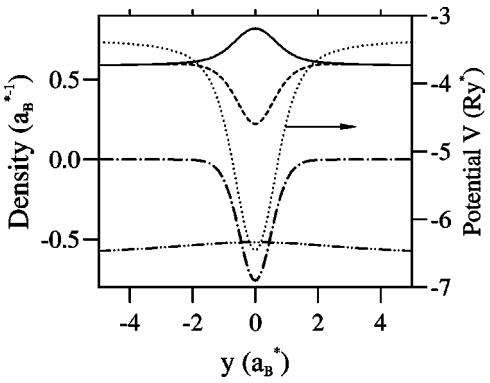

FIG. 15. Total electron density (solid), total density minus bound state (dashed), effective electrostatic potential $V_{eff}^{h}(y)$ (dotted), density of hole (dot-dashed), and density of gate charge (double-dot-dashed) versus y; same parameters as in Fig. 14.

the total conduction band density, exhibited in Fig. 15, peaks at $y=0$, this density minus that of the lowest state diminishes at the hole. Combined with the uniformly increasing background positive charge on the gate, this comprises a buildup of positive charge near the hole as U_{ext} and n_e are increased. Therefore an increased density of electrons produces an effectively antiscreening effect, which initially drives the electron closer to the hole and then admits a second and even a third bound electron. The hole eigenstate, meanwhile, is growing increasingly delocalized and the faster rise of its energy accounts for the increase of the overall energy (i.e., a decrease of the negative binding energy).

G. Combined results

Finally, in combining the results from Secs. II and III, we simply add the excitonic binding energy to the band gap calculated in the LDA for the translationally invariant wire. The results for this are shown in Fig. 6. Clearly the exchange-correlation and kinematic effects causing the BGR produce a redshift which is partially negated by the shift of the exciton binding energy due to screening. This is consistent with the notable insensitivity of the photoluminescence line position in optical experiments on quantum wires to either a photoexcited electron-hole plasma[4,5] or a gate-generated 1DEG.[13]

The dimensional dependence of BGR is a subject of considerable interest.[5] Within the ''free virtual state'' approximation to the Bethe-Salpeter equation,[32] renormalization is seen to stem from the screening of the exciton in combination with a phase-space filling effect. The relative importance of these effects in different dimensions has been discussed by Nojima.[33] Within the DFT context it is clear that, as noted above, the exciton binding energy can become very great for very narrow wires. We could argue then that the persistence of a redshift in 2D is at least in part due to the weaker bare exciton binding energy. It is not the case that the screening in 2D is less strong—it is stronger. It is merely that the range of the exciton energy from bare to fully screened (i.e., free e-h pair) is smaller in 2D. Hence the compensation for the exchange-correlation renormalization of the bands via exciton screening is weaker in 2D.

Interestingly, the approximate cancellation of exchange-correlation renormalization and exciton screening in 1D determined from our calculations is also consistent with recent calculations of the dynamically screened Bethe-Salpeter equation by Das Sarma and Wang[8] for wires with a two-component plasma, although the interpretation differs somewhat from that discussed here. While the tendency toward cancellation of BGR and excitonic screening is concluded in both studies, the most striking difference between the results of Ref. 8 and those here concerns the unbinding of the exciton, which, in an electron-hole plasma, is called the Mott transition. The authors of Ref. 8 estimate a merging of the exciton energy with the electron-hole band edge at around $n\sim 3\times 10^5$ cm^{-1}, where n is here of course the density of electrons *and* holes. Even in the simple one-electron static screening approximation they find a vanishing of the exciton binding energy with density. By contrast, we find that up to the highest density considered (3×10^6 cm^{-1}) the exciton remains bound. Assuming that both conclusions are correct, the implication is that it is the interaction *between* excitons that leads to their unbinding or, equivalently, their merging with the continuum.

In any case, the absence of a Mott transition, even for the single-component plasma that we study here, is of significant interest to both experimentalists and theorists. Our highest density (3×10^6 cm^{-2}) corresponds to slightly fewer than four electrons within the Bohr radius of the exciton ($\sim 1.2a_B^*$) and yet even at that density a bound exciton state still exists. What, then, would a Mott transition look like microscopically? The positively charged hole must, at any density, be surrounded by a cloud of negative charge, simply due to charge neutrality. Generally screening is thought of as the creation of electron-hole pairs at the Fermi surface, so one could imagine that at sufficiently high density the neutralizing electron cloud would shift from the bound state at the bottom of the Fermi sea to a cloud of ''Friedel'' electrons near E_F. However, since density functional theory is an effective single-particle theory and since an arbitrarily small attractive potential in one dimension binds an electron, the screening of the hole by the Fermi surface electrons would have to be essentially perfect in order to cancel the bound state. Whether this is an artifact of DFT which results, ultimately, from the local density approximation for exchange and correlation or whether it is a realistic physical manifestation of the anomalous behavior of 1D systems is not entirely clear. The experimental picture seems to show that exciton binding in 1D is far more robust than theories other than this one have predicted, lending some support to the physics behind our method. Thus the questions become how, if at all, does this picture break down and what is the actual criterion for the Mott transition in 1D? A theoretical approach to this would have to focus on the bistable point at which the neutralizing charge resides, with equal probability, on the bottom or the top of the Fermi sea.

IV. CONCLUSION

In conclusion, we have presented results of density functional calculations for the electronic structure of modulation

doped and gated T-shaped quantum wires for the case where the wire can be assumed to be translationally invariant. We have shown that the phenomenon of band-gap renormalization can be qualitatively and quantitatively understood within DFT. We have further employed a simplified model of a cylindrical quantum wire to examine the strength of the bound exciton state in the presence of a one-dimensional electron gas. We have normalized out the band structure problem here by defining the exciton binding energy as the difference between the total energy of the wire with a localized hole and that with the hole charge (and consequently all electrons) spread uniformly along the wire. We find that the variation of the exciton binding energy with density tends to cancel the band-gap renormalization, in agreement with recent experiments. Finally, we noted that, in this one-component plasma case, to the highest densities we have considered, no analog of the Mott transition, i.e., no unbinding of the electron and hole, occurs. This is therefore, to our knowledge, the first theoretical study that substantiates the well-known experimental findings on this issue.[5] Rather than unbinding, the orthogonality of the free electron states with those of the bound electron(s) leads to an antiscreening behavior such that as n_e increases a second (trion) and even a third (quadron) bound state forms at the hole.

In the future we hope to investigate the effect of dimensionality on the exciton physics by extending the calculation to include multiple 1D subbands.

ACKNOWLEDGMENTS

I wish to thank Werner Wegscheider, Stefan Sedlmaier, Sankar Das Sarma, and Elisa Molinari for helpful conversations.

*Email address: stopa@tarucha.jst.go.jp

[1] S. Glutsch, F. Bechstedt, W. Wegscheider, and G. Schedelbeck, Phys. Rev. B **56**, 4108 (1997).
[2] F. Rossi and E. Molinari, Phys. Rev. Lett. **76**, 3642 (1996).
[3] D. Brinkmann and G. Fishman, Phys. Rev. B **56**, 15 211 (1997).
[4] W. Wegscheider, L. N. Pfeiffer, M. M. Dignam, A. Pinczuk, K. W. West, S. L. McCall, and R. Hull, Phys. Rev. Lett. **71**, 4071 (1993).
[5] R. Ambigapathy, I. Bar-Joseph, D. Y. Oberli, S. Haacke, M. J. Brasil, F. Reinhardt, E. Kapon, and R. Deveaud, Phys. Rev. Lett. **78**, 3579 (1997).
[6] R. Zimmermann, K. Kilimann, W. D. Kraeft, D. Kremp, and G. Röpke, Phys. Status Solidi B **90**, 175 (1978).
[7] H. Haug and S. Schmitt-Rink, Prog. Quantum Electron. **9**, 3 (1984).
[8] S. Das Sarma and D. W. Wang, cond-mat/9905038 (unpublished).
[9] E. H. Hwang and S. Das Sarma, Phys. Rev. B **58**, R1738 (1998).
[10] See, for example, W. L. Bloss, J. Appl. Phys. **65**, 4789 (1989).
[11] C. Guillemot, Phys. Rev. B **31**, 1428 (1985).
[12] See, for example, Peter Fulde, *Electron Correlations in Molecules and Solids* (Springer-Verlag, Berlin, 1995), and references therein.
[13] The detailed growth pattern of the device that we model, and photoluminescence experiments in the presence of a gate-induced 1DEG, will be described in a companion publication: S. Sedlmaier, M. Stopa, G. Schedelbeck, W. Wegscheider, and G. Abstreiter (unpublished).
[14] For a discussion of our numerical techniques see M. Stopa, Phys. Rev. B **54**, 13 767 (1996).
[15] S. Das Sarma, R. Jalabert, and S. R. Eric Yang, Phys. Rev. B **39**, 5516 (1989); **41**, 8288 (1990).
[16] S. Schmitt-Rink, D. Chemla, and D. A. B. Miller, Adv. Phys. **38**, 89 (1989); R. Cingolani and K. Ploog, *ibid.* **40**, 535 (1991).
[17] D. M. Ceperley and B. J. Alder, Phys. Rev. Lett. **45**, 566 (1980).
[18] We employ the standard treatment of the band gap, taking in particular $E_g = 1512 + 1455\eta$ (meV) and $V_C = Q_e E_g$, where the band-gap offset parameter is taken as $Q_e = 0.6$. See M. Zachau, F. Koch, G. Weimann, and W. Schlapp, Phys. Rev. B **33**, 8564 (1986).
[19] M. Stopa, Phys. Rev. B **53**, 9595 (1996).
[20] U. Ekenberg and M. Alterelli, Phys. Rev. B **35**, 7585 (1987).
[21] G. Goldoni, F. Rossi, E. Molinari, and A. Fasolino, Phys. Rev. B **55**, 7110 (1997).
[22] A. Paassen, A. Zrenner, A. Efros, M. Stopa, J. Frankenberger, M. Bichler, and W. Wegscheider, Phys. Rev. Lett. **83**, 3033 (1999).
[23] G. Mahan, *Many-Particle Physics* (Plenum, New York, 1986).
[24] B. Vinter, Phys. Rev. B **26**, 6808 (1982).
[25] An alternative approach, taken, in the 2D case, by G. E. W. Bauer and T. Ando, Phys. Rev. B **31**, 8321 (1985), is to retain full translational invariance and include correlation of hole and electrons via a local approximation derived from the homogeneous 3D electron gas. The problem reduces thereby to one dimension. The authors justify this approach by arguing that the screened Coulomb interaction is short range and therefore momentum independent. Consequently vertex corrections turn out to be negligible. Whatever the virtues of this approach may be in a 2DEG, screening is certainly appreciably worse in 1D and it is very difficult to see the justification for abandoning the exciton effect altogether.
[26] J. M. Ziman, *Elements of Advanced Quantum Theory*, 4th ed., (Cambridge University Press, Cambridge, 1988), Sec. 5.3.
[27] M. Stopa, Y. Aoyagi, and T. Sugano, Phys. Rev. B **51**, 5494 (1995).
[28] S. Nojima, Phys. Rev. B **50**, 2306 (1994).
[29] J. D. Jackson, *Classical Electrodynamics* (Wiley, New York, 1975).
[30] G. D. Sanders and Y.-C. Chang, Phys. Rev. B **45**, 9202 (1992).
[31] R. Schilling and D. C. Mattis, Phys. Rev. Lett. **49**, 808 (1982).
[32] R. Zimmerman, Phys. Status Solidi B **146**, 371 (1988).
[33] S. Nojima, Phys. Rev. B **51**, 11 124 (1995).